PCCP

ROYAL SOCIETY OF CHEMISTRY

PAPER

View Article Online
View Journal | View Issue

Cite this: *Phys. Chem. Chem. Phys.*, 2026, **28**, 9604

Dynamics in renewable sourced random poly(trimethylene 2,5-furanoate-*co*-trimethylene suberate) copolymers: ambient-pressure fragility and compensation law in secondary relaxations

Agata Zubkiewicz, [a] Alejandro Sanz, *[b] Tiberio A. Ezquerra [c] and Anna Szymczyk *[d]

This article presents an experimental study on the relaxation dynamics in a series of random copolymers with optimum gas barrier properties based on bio-friendly monomers. The relaxation response of poly(trimethylene 2,5-furanoate-*co*-trimethylene suberate) copolymers is examined in the glassy and viscoelastic regime *via* frequency-domain spectroscopies (dielectric and mechanical). We report lower values of dynamic fragility, a dimensionless index introduced in 1985 [C. A. Angell, *Relaxations in Complex Systems*, ed. K. Ngai and G. B. Wright, National Technical Information Service, US Department of Commerce, Springfield, VA, 1985, p. 3; C. A. Angell, Formation of glasses from liquids and biopolymers, *Science*, 1995, **267**(5206), 1924–1935], in comparison to conventional polyesters used in industry, such as poly(ethylene terephthalate). We propose that this is consistent with their low permeability to gases. The sub-glass dynamics is complex and can be described by two local modes, β_1 and β_2, whereas for poly(trimethylene 2,5-furanoate) and the copolymer with the lowest suberate unit content we detect a single β relaxation. Our study reveals that sub-T_g relaxations obey the so-called compensation law, which is interpreted with respect to the multiexcitation entropy model by Yelon and Movaghar, and the more recent collective small displacements model.

Received 16th October 2025,
Accepted 14th March 2026

DOI: 10.1039/d5cp03981a

rsc.li/pccp

1 Introduction

Polymers are archetypal examples of glass-forming systems because of their intrinsic structural complexity at the microscopic level, where thermal fluctuations happen on a vast range of length and time scales.[1–3] However, one must note that chain connectivity and the presence of intramolecular barriers make polymers peculiar in comparison to molecular glass formers.[4] Despite these structural differences, glass-forming liquids in general and amorphous polymers in particular share common features, especially the lack of translational symmetry (for now we exclude semi-crystalline polymers). Glass-forming systems present a dynamic scenario that we can safely consider universal[5,6]: (1) vibrations, (2) fast relaxations on picosecond timescales, (3) Johari–Goldstein or "slow" β process, (4) the structural or α relaxation, which shows a super-Arrhenius temperature dependence, and (5) the temperature-independent Boson peak which is considered a characteristic feature of disordered solids.[5] Moreover, and depending on the chemical nature, some systems relax through the reorientation of a small part of the molecule (or segment when dealing with polymers). Thus, additional secondary relaxations may be observed, typically insensitive to pressure.[7]

Since a key unsolved question in this field is determining what truly governs the tremendous slowing down of transport coefficients at the proximity of the glass transition, the α relaxation is usually the process that receives more attention from the community.[8–10] That is why the dynamic arrest associated with the glass transition is in most cases characterized by the time scale of the α relaxation, τ_α. This relaxation deviates from the Arrhenius behaviour and such deviation is quantified using the concept of fragility. This dimensionless index, m, allows one to classify the liquid's behaviour during vitrification when the supercooled liquid is cooled (compressed[11]) and crystallisation is avoided[12–15]:

$$m = \left(\frac{\partial \log \tau_\alpha}{\partial (T_g/T)}\right)_{T=T_g} \quad (1)$$

[a] *Institute of Mathematics, Physics and Chemistry, Maritime University of Szczecin, Waly Chrobrego 1-2, PL 70-500 Szczecin, Poland*
[b] *Departamento de Ciencias y Técnicas Fisicoquímicas, Facultad de Ciencias, UNED, Las Rozas, Spain. E-mail: asanzparras@ccia.uned.es*
[c] *Instituto de Estructura de La Materia, IEM-CSIC, Madrid, Spain*
[d] *Department of Mechanical Engineering and Mechatronics, West Pomeranian University of Technology, Szczecin, Poland. E-mail: aszymczyk@zut.edu.pl*

Dynamic fragility is often estimated under isobaric conditions and is correlated with numerous physical properties of liquids and glasses, but in this article we focus on how the efficiency in polymer chain packing relates to the value of m. There are solid arguments that support the general idea that linear and flexible polymers adopt a compact packing, showing low values of fragility. Following the jargon used in this field, these systems would be classified as strong polymers. Meanwhile, those with high values of dynamic fragility are typically formed by stiff chains and in some cases with bulky pendant groups, resulting in poorly packed glasses or more open fluids in case the polymer is above the glass transition temperature.[16,17]

The aim of this paper is to present experimental results on the relaxation dynamics in a series of furanoate-based copolyesters. These are emerging materials due to their promising mechanical and gas-barrier properties. One must keep in mind that excellent gas-barrier performance is a stringent requirement for many packaging applications, such as beverage bottles. Here is where polymers based on 2,5-furandicarboxylic acid present a major advantage.[18–20] It is well known that gas permeation through polymers is highly dependent on their chain structure, aggregation, interchain interactions and degree of crystallinity.[21] All these factors together will determine the ability of the polymeric chains to adopt the most compact packing and ultimately the fraction of free volume. Since the latter is one of the factors controlling gas permeation, molecular mobility plays a key role in governing the relationship between physical properties and gas-barrier performance. This work presents results obtained mainly from mechanical spectroscopy (MS) and dielectric spectroscopy (DS) in novel fully bio-based poly(trimethylene 2,5-furanoate-*co*-trimethylene suberate) (PTFcoTSub) copolymers. Complementary analysis *via* differential scanning calorimetry (DSC) is also reported. Besides large-scale segmental dynamics, we observe sub-T_g relaxations for which we evaluate the corresponding enthalpic and entropic contributions *via* the Eyring formalism. Finally, we discuss tentative correlations between dynamic fragility and gas-barrier properties, segmental and local cooperativity, and the variations in configurational disorder during localized thermal fluctuations.

2 Experimental section

2.1 Materials and film preparation

The samples studied are fully bio-based random poly(trimethylene2,5-furanoate-*co*-trimethylene suberate) copolymers with aliphatic co-unit content in the range 0 to 25 mol%. These random PTFcoTSub copolymers were synthesized by a two-stage melt polycondensation method from dimethyl 2,5-furandicarboxylate (FDCA-DM, 99.8%, Matrix Fine Chemicals GmbH, Switzerland) and 1,3-propanediol (Susterra® PDO, 98%, DuPont Tate & Lyle) with dimethyl suberate (DMSub, 99%, Sigma-Aldrich Co.) in the presence of titanium(IV) butoxide (TBT, 97%, Sigma-Aldrich Co.) as the catalyst. In the first step, the reaction mixture was progressively heated for 2 h from 433 to 443 K under a nitrogen atmosphere. In the second step, a vacuum (18 Pa) was applied, and the temperature was increased up to 508 K. A detailed description of the synthesis along with chemical and physical characterization is presented in a paper published by some of the current co-authors,[22] confirming the randomness nature of the copolymers. The chemical structure is shown in Fig. 1. Details of the composition, molecular weight and polydispersity index are provided in Table 1. The values of thermal transitions and degree of crystallinity determined from the 1st heating traces at a standard rate of 10 K min^{-1} for the PTF and copolyesters, as well as representative DSC traces, are presented in Table 2 and Fig. 2. Measurements were made on a DSC F1 Phoenix instrument, which was calibrated with indium for the heat flow and temperature, while the heat capacity was evaluated using a sapphire standard. The samples (10 ± 0.2 mg), encapsulated in aluminum crucibles, were first cooled down to 213 K and then heated up to 498 K. Cold crystallisation temperature (T_{cc}) and melting temperature (T_m) were determined as the maximum/minimum of the exothermic/endothermic transitions respectively. The corresponding heat of fusion and heat of crystallisation were obtained from the total area of the endothermic and exothermic signals, respectively. Regarding T_g, the reported values were estimated at the midpoint of the jump in heat flow across the glass-to-liquid transition. Table 2 shows the average values from three measurements for each sample. The results reveal that, when stored at room temperature for one month, only the copolyester containing 25 mol% of TSub units undergoes crystallisation. PTF and the copolymers containing 5 and 15 mol% of TSub units remain amorphous. Previous research has shown that PTF and random PTFcoTSub copolymers do not undergo crystallisation during cooling at the standard rate of 10 K min^{-1}.[22] It was also observed that the crystalline structure in PTF and the copolymers containing 5 and 15 mol% of TSub units develops upon annealing at temperatures above 353 K. For copolymer $PTF_{75}coTSub_{25}$ no cold crystallisation occurred, but two melting endotherms were observed, at 335 K and the higher melting peak at 396 K. After annealing, the small endotherm at 335 K disappears. Annealed PTF and copolymers present melting peaks at lower temperatures next to the upper melting peak. As can be seen in panel (b) of Fig. 2, a small endotherm at 402 K is visible next to the endotherm at 449 K for PTF, and two peaks at 440 and 387 K are visible below

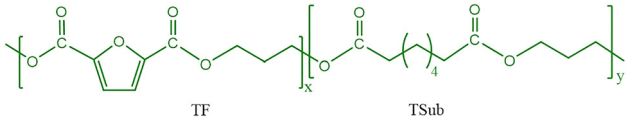

Fig. 1 Chemical structure of random poly(trimethylene 2,5-furandicarboxylate-*co*-trimethylene suberate) copolyesters.

Table 1 Chemical composition of PTFcoTSub copolymers and their molecular weight and polydispersity index

System	TSub in copolymer (mol%)	M_w (kg mol^{-1})	PDI
PTF	0	70	2.02
$PTF_{95}coTSub_5$	5	83	2.18
$PTF_{85}coTSub_{15}$	15	90	2.11
$PTF_{75}coTSub_{25}$	25	102	2.23

Table 2 Thermal transitions determined from 1st heating DSC scans (at 10 K min^{-1}) for PTF and PTFcoTSub random copolymers and the degree of crystallinity determined from DSC and X-ray measurements for samples before and after annealing

System	T_g (K)	T_{cc} (K)	ΔH_{cc} (J g^{-1})	T_m (K)	ΔH_m (J g^{-1})	x_c (%)	x_c (XRD) (%)
PTF	331 ± 2	402 ± 3	30.5 ± 0.6	446 ± 1	30.5 ± 0.5	0	0
PTF[a]	333 ± 1	—	—	449 ± 2	46.6 ± 1	32.9 ± 0.7	—
$PTF_{95}coTSub_5$	320 ± 1	405 ± 1	25.0 ± 0.3	440 ± 1	25.0 ± 0.5	0	0
$PTF_{95}coTSub_5$[a]	322 ± 1	—	—	441 ± 1	30.7 ± 0.4	21.64 ± 0.3	—
$PTF_{85}coTSub_{15}$	303 ± 1	391 ± 1	18.3 ± 0.5	424 ± 1	18.5 ± 0.5	0	0
$PTF_{85}coTSub_{15}$[a]	304 ± 1	—	—	426 ± 2	36.1 ± 0.3	25.4 ± 0.2	—
$PTF_{75}coTSub_{25}$	286 ± 1	—	—	335; 396 ± 1	6; 31 ± 1	26.1 ± 0.7	23.5
$PTF_{75}coTSub_{25}$[a]	288 ± 1	—	—	387 ± 1	32.0 ± 0.2	22.6 ± 0.7	—

[a] Annealed at 373 K for 1 hour. T_g – glass transition temperature; T_{cc} – cold crystallisation temperature; T_m – melting temperature; ΔH_{cc}, ΔH_m – enthalpy of cold crystallisation and melting, respectively; x_c – degree of crystallinity.

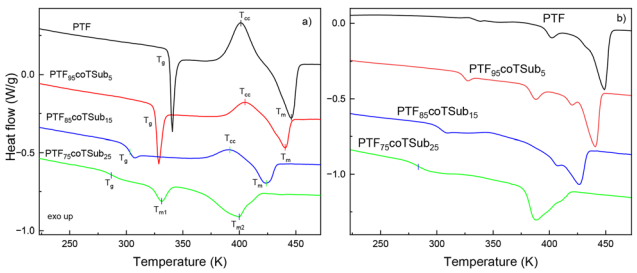

Fig. 2 Representative DSC traces obtained during the first heating scan at 10 K min^{-1} for PTF and PTFcoTSub copolymers: (a) before annealing and (b) after annealing at 373 K for 1 hour.

the peak at 440 K for copolymer $PTF_{95}coTSub_5$. Such multiple meting behaviour is typical for bulk crystallised PTF and its copolymers due to the polymorphic nature of 2,5-furan-based polyesters. A detailed study on the relationship between polymorphism and melting behaviour was performed by Righetti and coauthors.[23,24] Thus, depending on the crystallisation temperature, three different crystalline forms (α, α′ and β) can coexist, and crystal transformation from a less to a more perfect crystal structure occurs upon heating.[24]

For MS and DS experiments, dry granulates were melt pressed to ∼100–300 μm films by placing the samples between Kapton© layers at T_m + 20 K in three stages: pre-pressing (10 bar, 60 s), proper pressing (50 bar, 120 s) and cooling (20 bar, 60 s).

2.2 Mechanical spectroscopy (MS)

Dynamic-mechanical thermal analysis was carried out using a DMA 242 E/1/G Artemis (Netzsch, Selb, Germany) apparatus working in a bending mode. Samples were heated at a rate of 3 K min^{-1}, at a deformation frequency of 1 Hz, in the temperature range from 148 K to the melting point of the tested material. By using this technique we obtain the dynamic tensile modulus. This complex modulus provides information about the stiffness of the sample since the modulus describes how the material reacts to mechanical perturbations. For this particular method, the complex tensile modulus is expressed as $E^*(\omega) = E'(\omega) + iE''(\omega)$, with $E'(\omega)$ called the storage modulus (in phase with the applied strain) and $E'(\omega)$ being the loss modulus (out-of-phase contribution). The measurement error of the storage modulus was estimated to be within ±1–5%, depending on the temperature range.

2.3 Dielectric spectroscopy (DS)

Specimens for dielectric measurements were sputtered with gold, mounted between circular gold electrodes and measured using a spectrometer from Novocontrol Technologies (Alpha frequency analyzer). In this parallel plate configuration, the sample diameter was fixed to 20 mm, while the average sample thickness was different depending on the specimen, varying between 0.3 and 0.1 mm. The complex dielectric permittivity, $\varepsilon^*(\omega) = \varepsilon'(\omega) - i\varepsilon''(\omega)$, was acquired on heating, after cooling samples from room temperature to the starting temperature at a rate of 3 K min^{-1} approximately. Here, ω is the angular frequency, and ε' and ε'' are the real and imaginary parts respectively. The temperature was controlled by a nitrogen jet with 0.1 K precision during frequency sweeps from 10^{-1} to 10^6 Hz. We acquired isothermal spectra every 5 K from 123 to 373 K, that is, starting in the glass and ending above the glass transition temperature. A widely used alternative for analysing dipolar relaxations is the empirical Havriliak and Negami (HN) function. This model proposes a superposition of symmetric and asymmetric distribution of relaxation times[25,26]:

$$\varepsilon^*(\omega, T) = \varepsilon_\infty(T) + \frac{\Delta\varepsilon(T)}{\left[1 + (i\omega\tau_{HN}(T))^{b(T)}\right]^{c(T)}} \quad (2)$$

In most cases for temperatures below and above T_g, two terms are required to fit the relaxation processes. As an example, the following model function is used to describe spectra where both α and β relaxations are visible in the experimental frequency window:

$$\varepsilon^*(\omega, T) = \varepsilon_\infty(T) + \frac{\Delta\varepsilon_2(T)}{1 + (i\omega\tau_{HN2}(T))^{b_2(T)}} + \frac{\Delta\varepsilon_\alpha(T)}{\left[1 + (i\omega\tau_{HN\alpha}(T))^{b_\alpha(T)}\right]^{c_\alpha(T)}}, \quad (3)$$

Again, ω is the angular frequency of the applied field ($\omega = 2\pi\nu$), ε_∞ is the instantaneous or unrelaxed dielectric permittivity, $\Delta\varepsilon$ the dielectric strength of the relaxation, τ_{HN} is a characteristic relaxation time, b and c determine the symmetric and

asymmetric broadening of the relaxation peak respectively, while subscripts 2 and α stand for β_2 and α relaxations respectively. As indicated by the notation of eqn (2), all free parameters are temperature-dependent. We fitted the experimental spectra to a sum of Havriliak–Negami and/or Cole–Cole functions (when c is equal to 1) depending on the nature of the dynamics. We used a non-linear least square optimisation based on the Nelder–Mead simplex method.[27] The whole data analysis was carried out using MATLAB[28] scripts.

3 Results

3.1 Fixed frequency tensile mechanical modulus as a function of temperature

Fig. 3 illustrates the temperature dependence of the tensile storage modulus, tensile loss modulus and the mechanical loss tangent ($\tan\delta = E''/E'$) for the homopolymer PTF and copolymers before and after annealing at 373 K for an hour. Data were collected at a fixed frequency of 1 Hz. In all cases we observe two dynamic mechanical relaxations: α and β. At low temperatures, below 223 K, the imaginary part and tan δ curves show a single β relaxation associated with local motions of carboxyl groups attached either to the aromatic furan ring or to the aliphatic chain of TSub units in the amorphous phase. With increasing temperature, a rapid decrease in the storage modulus is observed due to exceeding the glass transition temperature, which is also manifested on the loss modulus and tan δ as a well-defined and intense maximum. As the molar content of TSub units increases, the glass transition peak shifts towards lower temperatures. Before annealing (Fig. 3a), after a rapid decrease in the real part because of the transition from the glassy to the rubbery state, a renewed increase in the modulus is visible, due to cold crystallisation of PTF chains.

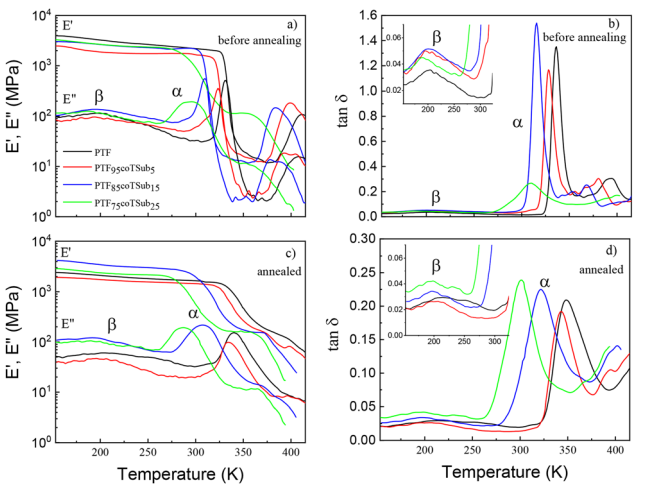

Fig. 3 Tensile storage modulus E', loss modulus E'' and tan δ as a function of temperature for a fixed frequency of 1 Hz. Data refer to PTFcoTSub copolymers before (a) and (b) and after (c) and (d) annealing at 373 K for an hour. Insets in panels (b) and (d) show zoomed-in versions of the temperature window where the β process is located.

The exception was copolymer $PTF_{75}coTSub_{25}$, initially semicrystalline as confirmed by previous calorimetric and X-ray diffraction studies.[22] Leaving aside the β process, this material shows two transitions, one from the glassy plateau to a lower-modulus plateau, and one when crystalline regions start melting and the whole material exhibits liquid-like behaviour. The onset of melting is also reflected as a sudden decrease in modulus just after cold-crystallisation in PTF, $PTF_{95}coTSub_5$ and $PTF_{85}coTSub_{15}$. Upon annealing, all samples developed semicrystalline structures, leading to broader and less intense thermal transitions, which is a hallmark of materials with a diminished fraction of mobile amorphous phase.

3.2 Local and segmental dynamics explored by DS

In this section we present new data on three members of the PTFcoTSub random copolymer series with a trimethylene suberate content of 5, 15 and 25 mol%. For comparison we also include data on poly(trimethylene 2,5-furandicarboxylate), PTF, which can be found elsewhere.[29] Fig. 4 illustrates how temperature and frequency govern the complex dielectric permittivity for $PTF_{85}coTSub_{15}$. This dielectric spectrum shows the typical evolution with temperature, where peaks (step-like shape in real part) move towards higher frequencies as temperature increases. The α relaxation dominates the signal at the time it enters the experimental frequency window around 298–303 K. At high temperatures, the intensity of the α relaxation drops due to cold crystallisation effects. The latter is also observed in PTF and $PTF_{95}coTSub_5$.[29] In contrast, the intensity of the α peak does not suffer any drop over the explored

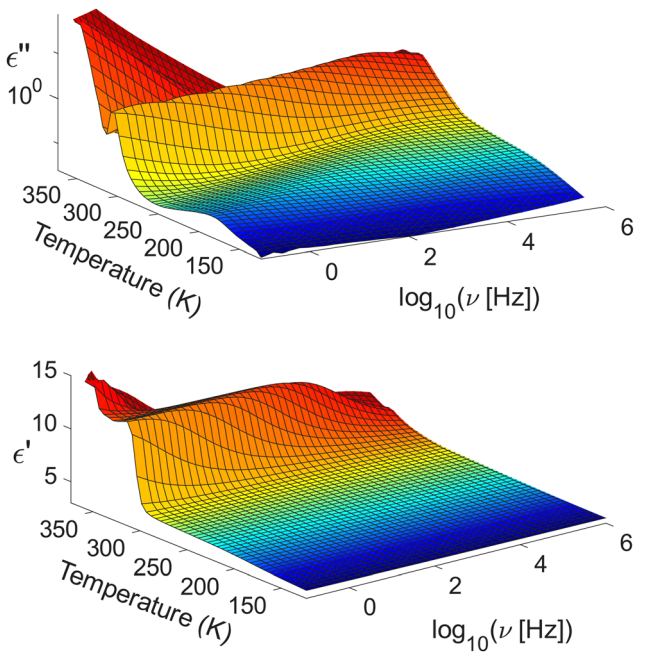

Fig. 4 Temperature and frequency (logarithm with base 10) evolution of the complex dielectric permittivity of poly(trimethylene 2,5-furandicarboxylate-*co*-trimethylene suberate) with 15 mol% content of suberate units ($PTF_{85}coTSub_{15}$). Top: Imaginary part. Bottom: Real part. Data spans from 123 to 373 K, every 5 K.

temperature for the copolymer with a 25 mol% of suberate units (see Fig. 7). At higher frequencies (lower temperatures), a broad maximum corresponds to a sub-T_g relaxation that can be decomposed into two symmetric modes in agreement with local fluctuations involving the furan ring and those with lower energy barriers associated with the suberate counit. These local relaxations are labeled β_1 and β_2 in the order of decreasing frequency or increasing temperature. Note that the increase of dispersion at low frequencies and high temperatures comes of ohmic and non-ohmic electric conduction, and interfacial polarization effects.[26,30] These contributions have been accounted for during fitting to obtain a meaningful decomposition of the raw data into the intrinsic relaxation modes.

3.2.1. α Relaxation. A full description of the dielectric spectrum above T_g requires us to account for the α and β relaxations. Interfacial polarization and dc-conductivity are integrated into the fitting routine but not discussed in the present paper (not shown in eqn (3)).[26,31] Fig. 5 illustrates simultaneous fitting of both real (bottom) and imaginary (top) parts of the complex dielectric function to eqn (3) at selected temperatures for $PTF_{85}coTSub_{15}$. The α peak dominates the spectrum, overlapping the much weaker high-frequency β_2 component. An interesting observation is the drop in intensity of the α relaxation at high temperatures due to cold crystallisation. In parallel, the α relaxation becomes broader and more symmetric in full agreement with partial crystallisation of the trimethylene 2,5-furanoate comonomer units.[22] This latter observation indicates that the nature of the structural dynamics is altered by the presence of crystals.[32]

In a first approximation one can assume that the system's response to the frequency-dependent field can be expressed as the superposition of individual responses. Such assumption of statistical independence in the frequency domain is reflected in the summation of terms of eqn (3), resulting in the full lines of Fig. 5. As an example, Fig. 6 shows the decomposition of raw data into individual components for $PTF_{85}coTSub_{15}$ at 323 K, 16 K above calorimetric T_g. Here one can recognize the α process, a secondary β_2 relaxation, dc-conductivity and the instantaneous value of the dielectric permittivity ε_∞. The inset in the top panel presents a log–log plot for the dielectric loss in order to highlight the location and broadening of the β_2 relaxation, which is partially overlapped by the high frequency tail of the α relaxation. Claiming the existence of this local process is supported by the data collected below T_g where process β_2 is fully resolved. Note that the sub-glass dynamics is discussed below. Excess of dielectric loss due to electric conductivity has been accounted for in the fitting routine by introducing the term $-i(\sigma/\varepsilon_0\omega^n)$, with σ being the dc-conductivity, the exponent $0.1 \leq n \leq 1$ governed by the mechanism of conduction and ε_0 is the permittivity of free space. In addition to that, at higher temperatures, an excess of dispersion at low frequencies is also detected in the real part of the permittivity. Given the semicrystalline nature of these polymers, it is plausible to state that this contribution is due to the blockage of free charges at interfaces. Therefore, in the analysis of the high-temperature spectra we have described these interfacial polarization effects as a single HN function. Note that this

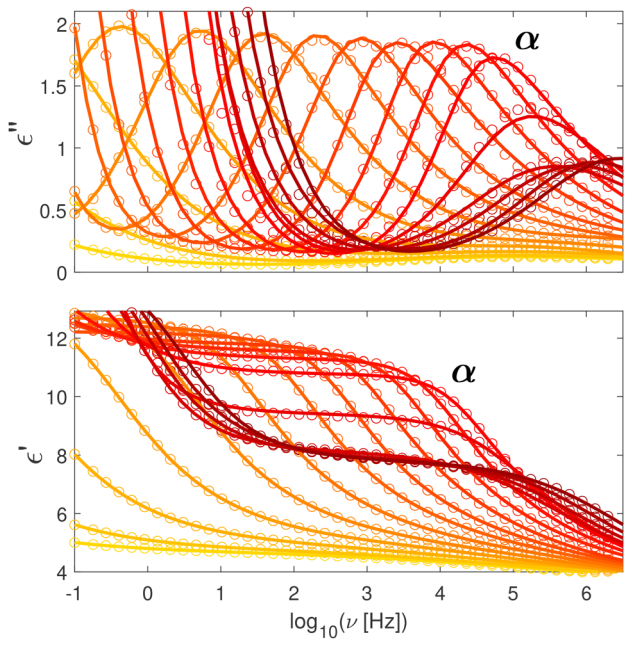

Fig. 5 Simultaneous fit of the complex dielectric permittivity using the Havriliak–Negami formalism for $PTF_{85}coTSub_{15}$ (eqn (3)). The main contribution to the signal corresponds to the structural or α relaxation. Data spans from 273 to 373 K, every 5 K. Top: Imaginary part. Bottom: Real part.

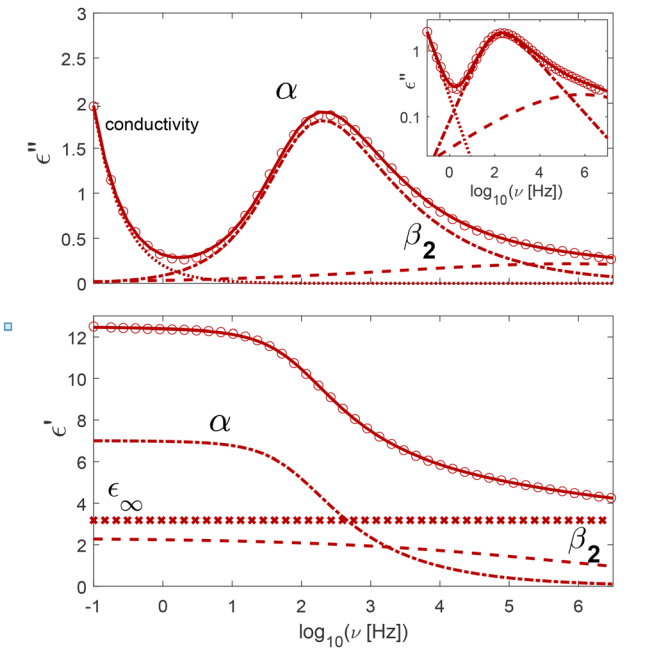

Fig. 6 Simultaneous fit of the complex dielectric permittivity to eqn (3) for $PTF_{85}coTSub_{15}$ at 323 K. Top: Imaginary part. Bottom: Real part. Only observed in the dielectric loss, a low-frequency contribution due to electrical conductivity is represented by the dotted line. Solid lines correspond to the total fit of the experimental data to the model function. The inset in the top panel shows the dielectric loss in a log–log representation.

assignment is merely pragmatic and not physically grounded. Migration and blocking of charges are ultimately the physical origin of the excess of permittivity in the low frequency flank detected at high temperatures.

As can be seen from Fig. 7 (panels a and b), the temperature-evolution of the dielectric strength for the α relaxation in $PTF_{75}coTSub_{25}$ exhibits a different behaviour. The intensity of the α process does not drop with temperature, but even increases slightly. This scenario is consistent with the presence of crystallinity as confirmed by X-ray scattering and DSC data.[22] Unlike what one sees in fully amorphous materials, the increase in temperature provokes that the intensity of the α relaxation for semicrystalline polymers often increases due to a progressive mobilization of a certain fraction of frozen disordered regions constrained by the crystals. This has been observed in several semicrystalline polymers.[26,29,33,34] It is important to bear in mind that the strength of dielectric relaxations is proportional to the density of free dipoles involved. Full lines in panels (a) and (b) of Fig. 7 represent the best fit of the experimental data to eqn (3) for temperatures above T_g. The bluish zone (low intensity/low temperatures) displays overlapped curves that correspond to the glassy state where we detected two local relaxations. In this region we fitted the whole spectrum using two Cole–Cole functions. But before discussing the nature of these β relaxations, we get back to the α process. The evolution with temperature of Havriliak–Negami shape parameters for semicrystalline $PTF_{75}coTSub_{25}$ differ from those shown by $PTF_{85}coTSub_{15}$ and the rest of the samples. In $PTF_{75}coTSub_{25}$, parameter b varies slightly with temperature from 0.35 to 0.5, while c is almost invariant with values close to 1. These are typical values for semicrystalline

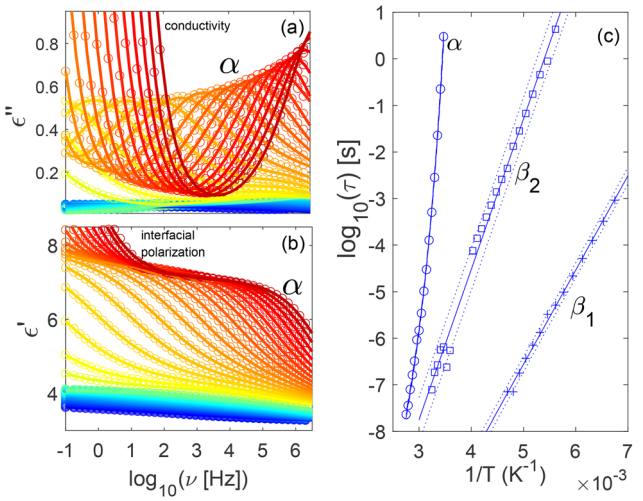

Fig. 7 Simultaneous fit of the complex dielectric permittivity using the Havriliak–Negami formalism for the random copolymer $PTF_{75}coTSub_{25}$. The main contribution to the signal corresponds to the α relaxation. Data spans from 148 to 363 K, every 5 K. (a) Imaginary part. (b) Real part. (c) Characteristic relaxation time with reciprocal temperature for α, β_1 and β_2 processes. Solid lines are fits to the VFT function for the α relaxation and to the Arrhenius equation for the two local modes, together with the corresponding 95% confidence intervals (dotted lines).

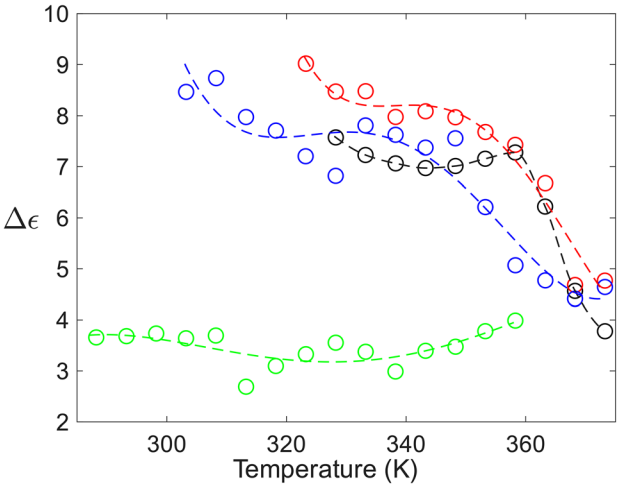

Fig. 8 Dielectric strength, $\Delta\varepsilon$, for the α relaxation obtained from fitting the experimental data to eqn (3). Dashed lines are guides to the eye. PTF (○), $PTF_{95}coTSub_5$ (○), $PTF_{85}coTSub_{15}$ (○) and $PTF_{75}coTSub_{25}$ (○).

polymers.[29,34–38] The behaviour in PTF, $PTF_{95}coTSub_5$ and $PTF_{85}coTSub_{15}$ is more complex since the shape parameters depend on both temperature and crystallisation. First, when samples remain fully disordered, b increases and c decreases upon heating. Then, when cold crystallisation takes place during further heating, b decreases and c increases, showing similar values as the ones for semicrystalline $PTF_{75}coTSub_{25}$. To remark how $PTF_{75}coTSub_{25}$ departs from the general behaviour, in Fig. 8 we present the temperature evolution of the dielectric strength for the α process. At low temperatures, semicrystalline $PTF_{75}coTSub_{25}$ presents lower values in comparison to the amorphous members of the series. In contrast, $\Delta\varepsilon$ for PTF, $PTF_{95}coTSub_5$ and $PTF_{85}coTSub_{15}$ first decrease in agreement with the theory of dielectric relaxation but at the onset of cold crystallisation there is a sharper drop due to the depletion of mobile dipoles.[29,37]

For building the relaxation maps we have used the average relaxation times as calculated analytically from the corresponding τ_{HN} values by following the standard approach.[26] Panel (c) of Fig. 7 illustrates the dependence of τ with reciprocal temperature for the α, β_1 and β_2 relaxations in $PTF_{75}coTSub_{25}$. As expected for the α process, governed in polymers by cooperative segmental motions, one observes a super-Arrhenius behaviour. In contrast, both secondary processes present a linear dependence from which it is possible to calculate the activation energy by linear regression.

Regarding the α relaxation, the data in Fig. 9 is consistent with the effect induced by the more flexible trimethylene suberate units on the values of T_g as shown in Table 2. By crossing the curves on isothermal lines, as the fraction of suberate units increases, there is a reduction in the structural relaxation time. As we demonstrated quantitatively in a previous study,[29] the Vogel–Fulcher–Tammann[39–41] expression is still one of the functions that best describes the temperature dependence of the α relaxation,[9,26,42,43] in particular when the pre-factor (limiting relaxation time at high temperatures) is

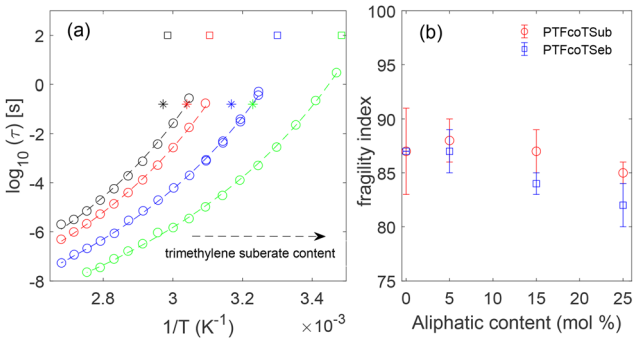

Fig. 9 (a) α relaxation time with reciprocal temperature for PTF (○), $PTF_{95}coTSub_5$ (○), $PTF_{85}coTSub_{15}$ (○) and $PTF_{75}coTSub_{25}$ (○). Dashed lines are fits to the VFT equation fixing the pre-exponential factor τ_0 to 0.01 ps. Star symbols correspond to the single frequency data obtained by mechanical spectroscopy. Empty squares represent T_g data by DSC, considering that jumps in heat capacity at the glass transition occur when the α relaxation is on a timescale of 100 s. (b) Dynamic fragility at constant atmospheric pressure *versus* trimethylene suberate and trimethylene sebacate content for PTFcoTSub and PTFcoTSeb[29] random copolymers. Dynamic fragility is calculated from $m = DT_0T_g0.4343/(T_g - T_0)^2$. See Section 3.2.1 for details about discrepancies in m when τ_0 is adjusted as a free parameter.

fixed to 10^{-14} s. Leaving aside considerations about whether or not there exists dynamic divergence at finite temperatures below T_g, the use of the VFT function is generally accepted for evaluating the steepness in the evolution of the α relaxation time with temperature when approaching T_g. In this phenomenological function, the α relaxation time is given by:

$$\tau = \tau_0 \exp\left(\frac{DT_0}{T - T_0}\right), \quad (4)$$

where τ_0 is a pre-exponential factor with phonon-like time scales, D is a strength parameter related to the dynamic fragility and T_0 is the Vogel temperature (divergence at $T = T_0$). The fits presented in panel (a) of Fig. 9 were obtained with values of τ_0 fixed to 10^{-14} s, while D and T_0 were adjustable parameters.[42,44,45] From VFT parameters it is possible to estimate the fragility index at ambient pressure using the relationship $m = DT_0T_g0.4343/(T_g - T_0)^2$, where T_g is the temperature at which the α relaxation time equals 100 s.[15] Values of VFT parameters are summarized in Table 3. It is important to remark that imposing a fixed value of 0.01 ps to τ_0 is physically reasonable and commonly used in this field.[42,45,46] Estimated values of the fragility index can be found in Fig. 9. Nevertheless, one may wonder how critical the differences in D and T_0 are in the case where τ_0 is allowed to vary as an adjustable parameter. As expected, fits optimized this way provide excellent results, with parameters also given in Table 3. There are significant differences in D that especially affect PTF and $PTF_{95}coTSub_5$. While fragility values decrease slightly with the suberate content when τ_0 is fixed to 0.01 ps, this reduction is stronger when τ_0 is a free parameter. When τ_0 is free to vary during fitting, m takes a value of around 112 for PTF, 103 for $PTF_{95}coTSub_5$, 93 for $PTF_{85}coTSub_{15}$ and 89 for $PTF_{75}coTSub_{25}$. This brings to the discussion the fact that the estimation of the steepness index is strongly dependent on the range of data considered when fitting. With the purpose of reducing the uncertainty to the possible minimum, we have performed the VFT fits only considering data where the maximum of the α relaxation is within the experimental window. This has supposed some limitation on the number of points near T_g, in particular for PTF and $PTF_{95}coTSub_5$. It is therefore plausible that the discrepancies in the VFT parameters with and without fixing τ_0 shown by these two systems are due to the limited range of data near T_g.

From the complex tensile modulus at 1 Hz, we have included mechanical α relaxation time in Fig. 9. These data deviate significantly from the curves obtained by DS. Such deviations between dielectric and mechanical α relaxation times are well known within linear response theory. Dielectric spectroscopy probes a retardation-type response (polarization build-up), whereas mechanical measurements in terms of the complex modulus correspond to a relaxation experiment (stress decay).

Table 3 Dynamic scenario of PTF and PTFcoTsub copolymers. Estimated parameters from VFT, Arrhenius, and Eyring equations (95% confidence bounds). Note that VFT parameters are given under fixed τ_0 conditions, but while also allowing this parameter to be adjusted during optimisation

Modes/parameters	PTF	$PTF_{95}coTSub_5$	$PTF_{85}coTSub_{15}$	$PTF_{75}coTSub_{25}$
α (MS)	Visible	Visible	Visible	Visible
α (DS)	Visible	Visible	Visible	Visible
β (MS)	Visible	Visible	Visible	Visible
β_1 (DS)	Absence	Absence	Visible	Visible
β_2 (DS)	Visible	Visible	Visible	Visible
VFT α (DS): D, T_0 (K), τ_0 = 0.01 ps	8.28 ± 0.50, 258 ± 4	8.16 ± 0.26, 255 ± 2	8.25 ± 0.20, 244 ± 1	8.53 ± 0.18, 229 ± 1
VFT α (DS): D, T_0 (K), τ_0[a] (s)	4.05 ± 0.8, 282 ± 6, 6.76×10^{-12} ×/÷4.8	5.3 ± 0.3, 269 ± 2, 5.01×10^{-13}×/÷1.61	7 ± 1, 249 ± 6, 4.68×10^{-14}×/÷5.5	7.5 ± 1, 234 ± 4, 3.24×10^{-14}×/÷3.4
Arrhenius β_1: ΔE (kJ mol^{-1})	—	—	36.6 ± 2.6	38.8 ± 2.6
Arrhenius β_2: ΔE (kJ mol^{-1})	51.3 ± 0.4	54.8 ± 1.3	59.7 ± 1.1	61.9 ± 1.1
Eyring β_1: ΔH (kJ mol^{-1}), ΔS (J K^{-1} mol^{-1})	—	—	35.1 ± 0.1, 57.8 ± 5.4	37.3 ± 0.1, 70.4 ± 3.4
Eyring β_2: ΔH (kJ mol^{-1}), ΔS (J K^{-1} mol^{-1})	49.4 ± 0.1, 32.1 ± 1.5	52.8 ± 0.1, 45.5 ± 3.3	56.2 ± 0.1, 57.5 ± 6.2	58.4 ± 0.2, 75.1 ± 6.1

[a] Confidence interval for τ_0 is defined as [estimate·F, estimate/F].

For a single characteristic process, the ratio between the retardation and relaxation times reflects the change in susceptibility between the short-time (solid-like) and long-time (liquid-like) limits, *i.e.*, the relaxation strength. Therefore, characteristic times obtained from dielectric and mechanical experiments may differ by up to a factor comparable to the step in mechanical compliance.[47,48] This observation is by no means surprising when dealing with a specific dynamic process when it is resolved by different methods that might show distinct manifestations of identical or similar underlying dynamic mechanisms. We also include values of τ_α determined from calorimetry. A fair approximation that is often assumed relates the temperature at which the jump in heat capacity during the glass-to-liquid transition takes place at standard rates to values for the dielectric α relaxation around 100 s.

3.2.2. Secondary relaxations. In the following we discuss the two types of secondary relaxations observed in these copolymers. To lay the grounds of the discussion, we first summarize the dynamic scenario for each sample in Table 3. PTF and $PTF_{95}coTSub_5$ exhibit a single β relaxation which is resolved in both mechanical and dielectric spectroscopy. For the particular case of PTF, this is in agreement with previous reports.[45,49] By contrast, for copolymers with a higher fraction of TSub units, we observe two well-resolved β relaxations by DS, but just one in the mechanics. Following the general trend, the observed secondary processes are weaker in relaxation strength than the α process since these secondary relaxations arise from localized reorientations of small parts of the macromolecular chains.[9,26,50–52] To illustrate graphically what is mentioned above, in Fig. 10 we present data below T_g for the whole series. Two symmetric relaxations fit the spectrum of both $PTF_{85}coTSub_{15}$ and $PTF_{75}coTSub_{25}$, while using just one asymmetric relaxation we got reasonable fits for PTF and $PTF_{95}coTSub_5$ with the exception of deviations in the dielectric loss at high frequencies. In these two latter cases we employed a HN function due to the asymmetric broadening at very low temperatures, such as the data at 193 K displayed in Fig. 10. Here, the HN shape parameters *b* and *c* are 0.63 and 0.25, respectively, for PTF. As temperature rises, *b* decreases and *c* increases becoming the relaxation fully symmetric or simply described by a Cole–Cole equation. Similar behaviour as temperature goes up is exhibited by $PTF_{95}coTSub_5$, with values for *b* and *c* of 0.62 and 0.14 respectively at 193 K. One may wonder whether we could have included another function at high frequencies to fit the spectra for $PTF_{95}coTSub_5$. We decided to skip this option considering the following points: (1) the real part (more intense and less subjected to uncertainties) is well described by just one relaxation; (2) unlike what is observed for $PTF_{85}coTSub_{15}$ and $PTF_{75}coTSub_{25}$, the signal excess at high frequencies in panel (c) of Fig. 10 does not evolve into a well-defined maximum or even shoulder when temperature decreases as demonstrated by the raw data at a temperature of 168 K (pink line in Fig. 10). It is important to note that for $PTF_{85}coTSub_{15}$ and $PTF_{75}coTSub_{25}$, two symmetric relaxations can fit the spectrum in the glassy sate, that is, the values of *c* were fixed to 1 for both the fast (β_1) and slow (β_1) relaxations.[29]

As expected for localized relaxations, the variation with reciprocal temperature of the average relaxation time shows a linear trend. An example of such behaviour can be found in Fig. 7. Thus, by fitting the temperature dependence of the β

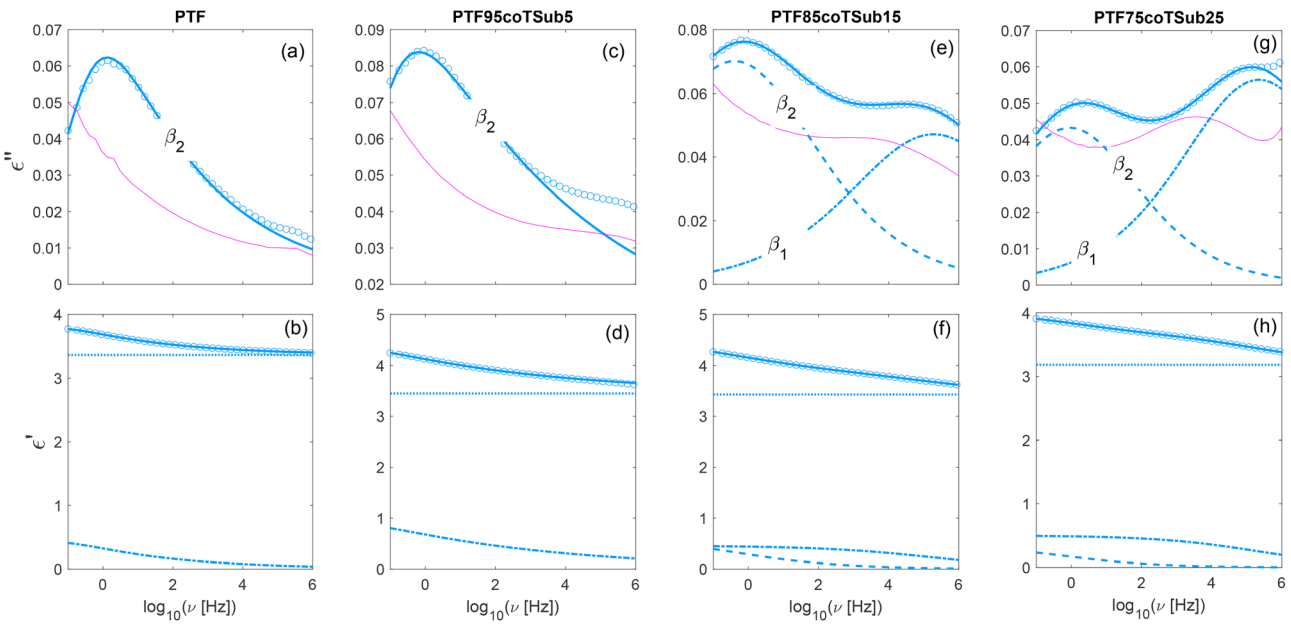

Fig. 10 Two separate modes (β_1 and β_2 in the order of decreasing frequency) contribute to the secondary relaxation for $PTF_{85}coTSub_{15}$ (panels e and f) and $PTF_{75}coTSub_{25}$ (panels g and h), while a single β_2 is resolved for PTF (panels a and b) and $PTF_{95}coTSub_5$ (panels c and d). Data correspond to a temperature of 193 K. Fast (β_1) and slow (β_2) secondary relaxations are denoted by the dash-dotted and dashed lines respectively. The dotted lines in the real part correspond to ε_∞. For comparison, the pink lines represent raw data at 168 K. In all cases the β processes are described as Cole–Cole functions with the exception of the β_2 relaxation for PTF and $PTF_{95}coTSub_5$ which are fitted using HN functions.

relaxation times to the Arrhenius function, $\tau = \tau_\infty \exp\left(\frac{E_a}{RT}\right)$,[29] we have estimated the apparent activation energies, which are collected in Table 3. We reported similar values for a family of related copolyesters based on PTF and trimethylene sebacate units (PTFcoTSeb).[29] It is therefore straightforward to assign the β_1 relaxation to the local reorientation of dipoles involving the ester groups of the trimethylene suberate units, while the β_2 relaxation is attributed to the ester group of trimethylene 2,5-furanoate units. The higher energy barrier shown by β_2 is consistent with the restriction imposed by the furan rings to the configurational reorientation of the ester groups. All these arguments would explain why neither PTF nor $PTF_{95}coTSub_5$ exhibit the β_1 relaxation.[29,49] Taking into account the chemical structure of these copolymers, we thus assign the microscopic origin of the observed secondary relaxations to localized intra-segmental reorientations along the backbone.

An interesting point here is the increase of activation energy with the content of TSub units for the β_1 and β_2 relaxation. Although exhibiting a less pronounced trend, a similar observation was reported in our previous study on PTFcoTSeb copolymers, that is, the increase of the energy barrier for the β_2 process with the fraction of trimethylene sebacate co-units.[29] This might appear contradictory with the higher mobility of the aliphatic TSub or TSeb repeat units but one must take into account other effects such as the greater efficiency in chain packing for flexible aliphatic backbones and the presence of crystalline domains for the particular case of $PTF_{75}coTSub_{25}$. All these factors can ultimately modify the potential energy landscape. Modifications of the local environment at the microscopic level would thus determine the height of the energy barrier that these localized motions must overcome. Regarding the influence of low-T_g comonomers on the activation energy of β relaxations linked to carbonyl groups, one can find random copolymers sharing common traits to the ones we report here,[53] while others do not.[54]

In this work we take a step forward to understand the microscopic implications of the observed secondary relaxations by applying the so-called Eyring formalism based on the transition-state theory.[55] According to this approach, the relaxation time reads as follows:

$$\frac{1}{\tau} = \frac{k_B T}{h} \exp\left(\frac{\Delta S}{k_B}\right) \exp\left(-\frac{\Delta H}{k_B T}\right), \qquad (5)$$

with k_B and h the Boltzmann and Planck constants, respectively, ΔS is the activation entropy and ΔH is the activation enthalpy of the corresponding β relaxation. This function can be linearized by considering the dependence of the natural logarithm of $(\tau T)^{-1}$ with reciprocal temperature. Such plots give straight lines as displayed in panel (a) of Fig. 11, with a slope related to ΔH and an intercept proportional to ΔS. According to thermodynamics, ΔH and ΔS combine to determine the change in Gibbs free energy in going to the transition state,[55,56] $\Delta G = \Delta H - T\Delta S$. In Table 3 we collect the values of ΔH and ΔS. The variations in entropy during the transition to overcome the energy barrier are positive in all cases. This implies that

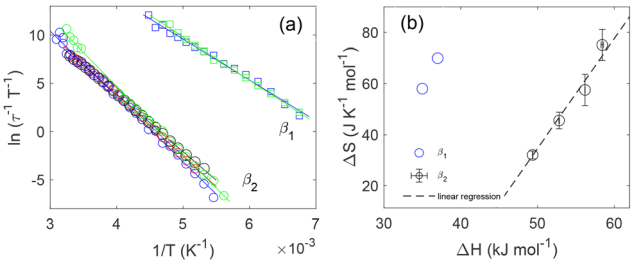

Fig. 11 (a) Plots of $\ln(\tau T)^{-1}$ as a function of reciprocal temperature for β_1 and β_2 relaxations, together with their corresponding fits to eqn (5) in its linear form. (b) Compensation law plots for β_1 and β_2 relaxations in PTF and PTFcoTSub copolymers. The slope of the dotted line (β_2 relaxation) is a reciprocal temperature which provides insight into the strength of the compensation effect.

localized rearrangements in both furanoate and suberate units induce an increase of configurational entropy. In other words, the density fluctuations behind both β_1 and β_2 to some extent present internal coupling or correlation and promote disorganization of the local environment. Thus, local motions in glassy PTF and PTFcoTSub copolymers lead to an increase of the microscopic heterogeneity.[57,58] Note that a general picture and meaningful definition of cooperativity is still missing, so establishing a direct link between cooperativity and dynamic heterogeneity is not straightforward.[6,59] What is confirmed from the data shown in Table 3 is that the activation enthalpy for the secondary relaxations does correspond to the apparent energy barrier determined from the Arrhenius equation. For the particular case of β_2, which is resolved for the whole series, ΔH increases with the fraction of trimethylene suberate units. Such a scenario made us consider a possible linear dependence between enthalpy and entropy during the activation of β_2 relaxation. This compensation effect is confirmed in panel (b) of Fig. 11 where a simple linear regression highlights the positive relationship between ΔS and ΔH. The compensation effect is a universal phenomenon that has been observed in a multitude of thermally activated physical, chemical and biological processes.[56,60–64] This correlation is basically equivalent to stating that the logarithm of the pre-exponential factor in the Arrhenius equation depends linearly on the apparent activation barrier.

4 Discussion

The segmental dynamics of these random copolymers accelerates with the increase in the TSub unit fraction. In parallel, we report a slight decrease of the dynamic fragility as the ratio of TSub to PTF units increases, especially for the last member of the series, $PTF_{75}coTSub_{25}$. A more pronounced trend is observed when τ_0 is allowed to vary during optimisation. Although the reported decrease in fragility is subjected to some uncertainty given the error bars and the influence of the constraints on τ_0, this observation is in full agreement with the general view that smooth, compact and linear polymeric backbones allow more efficient chain packing. By contrast, stiff

chains and/or the presence of bulky/stiff side groups would lead to a high packing frustration, thus resulting in more fragile glass formers. The increase in flexibility due to the presence of TSub units favor the adoption of a more compact chain packing at the glass transition temperature, which, together with intra- and inter-molecular interactions such as hydrogen bonds and π–π stacking of the furan rings, may be related to the exceptional barrier properties of these copolymers.[22] We reported similar results for random copolymers based on poly(trimethylene 2,5-furanoate) and poly(trimethylene sebacate), which were prepared *via* similar routes.[29,65]

As mentioned above, the temperature dependence of the α relaxation time at the proximity of T_g is usually considered a key element to understand the process of glass formation. As we do in the present article, a common way to characterize quantitatively this steepness is through the concept of fragility. This index, introduced by Angell four decades ago,[12,14] gives information about the particle cooperativity (molecular or segmental) and is then often used to determine empirical correlations with a multitude of physical properties of glasses and liquids.[1,59,66,67] But before moving on, the reader must note that the slowing down of the structural relaxation when supercooled liquids approach T_g is controlled simultaneously by temperature and density.[11,68–72] This must be taken into account when searching for correlations between fragility and other properties as temperature and density are also imprinted in ambient-pressure fragility. Moreover, the dynamic fragility is frequently interpreted somewhat loosely since its value is often expressed under different conditions such as (i) the value of the α relaxation time at which it is estimated, (ii) the robustness of VFT fitting and value of the pre-exponential factor, (iii) the thermodynamic path (process at constant pressure or constant volume) and (iv) the overlooked presence of crystallinity in materials with fast crystallisation rates.

In our previous paper,[29] we speculated about a possible connection between fragility at atmospheric pressure and the permeability of polymers to gases. Gas permeation of polymeric materials is a rather complex process in which several factors are involved, namely chain structure, macro-scale morphology, degree of crystallinity, chain and crystal orientation, inter-chain interaction, volume fraction and the physical affinity between the corresponding gas and the polymer. All these factors are behind the solubility and diffusivity of the molecule that, in the end, will govern the permeability of polymeric membranes.[73] Considering that molecular transport through polymers is favored by the presence of vacant spaces, either static or created by conformational jumps, it is expected that molecular mobility and packing frustration might be two excellent features to predict the permeability to gases in polymers.[22,65,74] And here is when fragility comes into play. There are now solid arguments to postulate fragility as a concept that is intrinsically linked to the extent of cooperative motion and free volume. In simple words and all determined by the chemical structure and molecular mass, both free volume and the extent of cooperative motions at the glass transition tend to increase the values of dynamic fragility. A theoretical approach that tries to rationalize this problem is the generalized entropy theory of polymer glass formation.[75] Under this framework, Xu and coworkers[46] have recently reported interesting calculations of the configurational entropy as a function of molecular mass and chain stiffness, concluding that the fragility in polymers at the segmental scale increases with the degree of packing frustration in full agreement with previous empirical observations that found high values of fragility for polymers with stiff and complex structures.[17,59,76–79]

The series of copolymers we study here presents intermediate values of fragility if we set the limits around 40 for poly(isobutylene) and close to 200 in the case of poly(ether imide) and poly(vinyl chloride).[29] Even values higher than 350 have been reported for the super-fragile poly(ether ether ketone).[35] In the context of this extremely broad range in values of fragility, the dependence of m with either suberate or sebacate aliphatic co-units is almost insignificant. It is also important to note that the copolymer with 75% mole fraction is semicrystalline in both series. The lower values of the steepness index in $PTF_{75}coTSub_{25}$ can plausibly be explained by the presence of crystals,[80] which, together with a higher fraction of linear and flexible chains, alter the energy landscape. Accordingly, the density fluctuations behind the α process will occur over an inhomogeneous environment providing different characteristic relaxation times and modifying the shape of the activation plot.[38] A recent work on block copolymers based on poly(lactic acid) and poly(butylene succinate) shows a similar general behaviour.[81] What we already proposed in our previous article is that amorphous polymeric matrices with low transmission to gases are expected to have low or intermediate fragility indices, while fragile and super-fragile polymers should present poor barrier properties. A recent empirical proof demonstrates that organic materials (molecules and polymers) with higher free volume at T_g tend to be more fragile.[82] Our approach is backed up by the reasoning offered. Of course, since the mechanism of gas migration through polymer membranes is rather complex and considering that dynamic fragility still remains a controversial concept, additional research is needed to validate our hypothesis.

We have seen that the family of copolymers PTFcoTSub show β_2 relaxation with values of activation entropy and enthalpy which have a linear relationship. Numerous thermally activated chemical and physical processes that obey the Arrhenius equation are also characterized by holding a linear dependence between the logarithm of the pre-exponential factor and the apparent energy barrier.

Whereas one can find in the literature several ways to name this empirical rule, here we will just utilize compensation law or compensation effect.[62] For those processes that present linear proportionality between the variation of entropy and enthalpy during the transition, a convenient approach to disentangle both contributions is the use of the Eyring equation (eqn (5)). Following this procedure, we were able to prove the proportionality of such quantities as displayed in panel (b) of Fig. 11. A widely accepted picture of relaxations from a microscopic perspective implies that particles remain trapped within

local basins of the energy landscape vibrating at frequencies that would correspond to the pre-exponential factor of the Arrhenius equation.[83] Eventually, while particles vibrate during this sort of confinement imposed by their neighbors, they will be able to explore other basins by overcoming the corresponding energetic barrier. Ultimately, the probability of these jumps will determine the characteristic relaxation time. Thoms and Napolitano observed that the slow Arrhenius process (SAP) follows the compensation law for numerous amorphous and semicrystalline polymers.[63] Following the line of thought of these authors, our results indicate that the β_2 relaxation in PTFcoTSub copolymers to some extent is cooperative, or at least collective in the sense of a coordinated and simultaneous action of low energy single excitations.[63,84] As the topography of the energy landscape is transformed by the presence of more TSub units within the copolymer, the energy barrier to be overcome by the motions underlying the β_2 mode increases. Yelon and Movaghar proposed a theoretical explanation of the compensation law.[85,86] Under this theory, if the activation energy is high compared to individual excitations of the system, many of them must participate for the transition to take place. Therefore, the number of excitations within the relaxation volume is governed by the height of the barrier. Since the entropy depends on the density of microstates involved in these excitations, ΔS will increase as ΔH increases. This approach provides a useful framework to investigate the physical origin of the compensation law associated with the β_2 process in PTFcoTSub copolymers.

Furthermore, the collective small displacements model (CSD) arises as an alternative framework that may contribute to the comprehension of the compensation effect reported in the present article.[87] White and coauthors propose this model to rationalize at the molecular level the slow Arrhenius process, which is mainly detected by dielectric spectroscopy.[63] According to this model, coordinated although small displacements of single particles (segments in the case of polymers) can lead to effective reshaping of local structures without the necessity of cage breaking. The activation of the corresponding sub-region is a previous step for the reorganization of the local structure to occur. Such activation takes place *via* transfer of thermal energy from the surroundings, increasing the entropy of the subsystem. According to this picture, an effective average of the dependence of entropy with enthalpy, dS/dH, is related to the ratio of activation entropy and activation enthalpy for individual segments, $\Delta s/\Delta h$. Note that dS/dH must be an effective reciprocal temperature. The CSD model identifies $\Delta s/\Delta h$ with $\Delta S/\Delta H$, in such a way that the slope of the ΔS *vs.* ΔH plot determines $1/T_{00}$, with T_{00} a parameter that quantifies the strength of the compensation effect. We are fully aware of the fundamental differences between SAP and β relaxations (for instance, location in the activation plot and energy barrier) that may question the utilization of arguments of the CSD model for a better understanding of the β_2 process reported here. Nevertheless, note that both SAP and elementary β relaxations are thought to occur without escaping the cage. For the particular case of the PTFcoTSub series, the value of T_{00} for β_2 relaxation is obtained from the linear regression displayed in panel (b) of Fig. 11. The corresponding slope yields a value of 233 K for T_{00}, with the following lower and upper 95% confidence bounds [170,370] (R_{sq} = 0.985). This gives $k_B T_{00}$ = 1.9 ± 0.8 kJ mol^{-1} ($\approx$20 meV). $k_B T_{00}$ is related to the energy of single excitations in the Yelon–Movaghar model, also known as the Meyer–Neldel energy, and in this particular case can be associated with local intra-segmental interactions. We observe large uncertainties in T_{00}, which may arise from experimental scatter and the intrinsic heterogeneity of polymers. Consequently, here the compensation law must be interpreted with caution. Nevertheless, from the error bars in panel (b) of Fig. 11, we firmly believe there exists a compensation law and the observed linear dependence is not just a false effect.

5 Summary and conclusions

We have shown that the family of random copolymers poly(trimethylene 2,5-furanoate-*co*-trimethylene suberate) exhibits rich dynamic behaviour as explored using dielectric and mechanical spectroscopies. Intermediate values of dynamic fragility are reported, decreasing slightly with the fraction of trimethylene suberate units. In comparison to commercially available polymers used in the packaging industry, these copolymers present improved gas barrier properties. In parallel, they show lower values of dynamic fragility. We argue that this behaviour is due to a lower degree of packing frustration, in other words, because of a more efficient chain packing. Our claim is that dynamic fragility might be a useful indicator to predict the gas transport properties of polymeric matrices, which deserves more tests in the future.

In addition, we present results that support the existence of compensation effects for the secondary process that appears at lower frequencies. Unfortunately, this compensation effect could not be explained in full for the high frequency secondary relaxation, β_1. The linear correlation between entropy and enthalpy for β_2 is interpreted according to the theoretical model proposed by Yelon and Movaghar. We conclude that as the topography of the energy landscape changes with the increase of TSub units, the entropy of activation for the β_2 relaxation increases as the density of microstates involved in the fluctuations becomes higher. We also propose a compelling interpretation of the compensation law observed in the β_2 process, based on the recently developed CSD model. This framework opens new avenues for a deeper understanding not only of the mechanism underlying the so-called SAP process, but also of that associated with elementary secondary relaxations.

Author contributions

Agata Zubkiewicz: conceptualisation; investigation; writing – review & editing. Alejandro Sanz: conceptualisation; formal analysis; writing – original draft. Tiberio Ezquerra: conceptualisation; investigation; funding acquisition; writing – review & editing.

Anna Szymczyk: conceptualisation; investigation; writing – review & editing.

Conflicts of interest

There are no conflicts to declare.

Data availability

The main experimental data reported in our manuscript are available through the repository ''Materials Data Facility''.[88] These data were collected at the Institute for the Structure of Matter that belongs to the Spanish Council for Higher Research (CSIC, Madrid, Spain). For more details, please contact Prof. Tiberio A. Ezquerra (t.ezquerra@csic.es).

Acknowledgements

TAE thanks the Spanish Ministry of Science and Innovation (MCIN) and the State Research Agency (AEI) for funding through projects PID2022-138635NB-I00 and TED2021-129845B-I00 (MCIN/AEI/10.13039/501100011033), co-funded by the European Regional Development Fund (ERDF, ''A way of making Europe'').

Notes and references

1 P. Lunkenheimer, A. Loidl, B. Riechers, A. Zaccone and K. Samwer, *Nat. Phys.*, 2023, **19**, 694–699.
2 P. Lunkenheimer and A. Loidl, *Macromolecules*, 2025, **58**, 3547–3553.
3 P. Szymoniak, F. Juranyi, M. Kruteva, R. Zorn and A. Schönhals, *Macromolecules*, 2025, **58**, 7112–7123.
4 J. Colmenero, *J. Phys.: Condens. Matter*, 2015, **27**, 103101.
5 B. Frick and D. Richter, *Science*, 1995, **267**, 1939–1945.
6 M. D. Ediger, C. A. Angell and S. R. Nagel, *J. Phys. Chem.*, 1996, **100**, 13200–13212.
7 K. L. Ngai and M. Paluch, *J. Chem. Phys.*, 2004, **120**, 857–873.
8 J. C. Dyre, *Rev. Mod. Phys.*, 2006, **78**, 953–972.
9 K. Niss and T. Hecksher, *J. Chem. Phys.*, 2018, **149**, 230901.
10 J. C. Dyre, *J. Phys. Chem. Lett.*, 2024, **15**, 1603–1617.
11 C. M. Roland, S. Hensel-Bielowka, M. Paluch and R. Casalini, *Rep. Prog. Phys.*, 2005, **68**, 1405.
12 C. Angell, Strong and fragile liquids, in *Relaxations in Complex Systems*, ed. K. Ngai and G. B. Wright, National Technical Information Service, US Department of Commerce, Springfield, VA, 1985, pp. 3–11.
13 C. Angell, *J. Non-Cryst. Solids*, 1991, **131–133**, 13–31.
14 C. Angell, *Science*, 1995, **267**, 1924–1935.
15 R. Bohmer, K. L. Ngai, C. A. Angell and D. J. Plazek, *J. Chem. Phys.*, 1993, **99**, 4201–4209.
16 D. M. Colucci and G. B. McKenna, *MRS Proc.*, 1996, **455**, 171.
17 A. P. Sokolov, V. N. Novikov and Y. Ding, *J. Phys.: Condens. Matter*, 2007, **19**, 205116.
18 A. F. Sousa, C. Vilela, A. C. Fonseca, M. Matos, C. S. R. Freire, G.-J. M. Gruter, J. F. J. Coelho and A. J. D. Silvestre, *Polym. Chem.*, 2015, **6**, 5961–5983.
19 E. de Jong, H. R. A. Visser, A. S. Dias, C. Harvey and G. J. M. Gruter, *Polymers*, 2022, **14**, 943.
20 K. Loos, R. Zhang, I. Pereira, B. Agostinho, H. Hu, D. Maniar, N. Sbirrazzuoli, A. J. D. Silvestre, N. Guigo and A. F. Sousa, *Front. Chem.*, 2020, **8**, 585.
21 G. Robertson, *Food packaging: Principles and Practice*, 3rd edn, CRC Press, 2016.
22 A. Zubkiewicz, A. Szymczyk, J. Dryzek, Z. Rozwadowski, R. J. Sablong, M. Soccio, G. Guidotti, V. Siracusa and N. Lotti, *Eur. Polym. J.*, 2025, **223**, 113673.
23 M. C. Righetti, P. Marchese, M. Vannini, A. Celli, F. Tricoli and C. Lorenzetti, *Thermochim. Acta*, 2019, **677**, 186–193.
24 M. C. Righetti, P. Marchese, M. Vannini, A. Celli, C. Lorenzetti, D. Cavallo, C. Ocando, A. J. Müller and R. Androsch, *Biomacromolecules*, 2020, **21**, 2622–2634.
25 S. Havriliak and S. Negami, *Polymer*, 1967, **8**, 161–210.
26 F. Kremer and A. Schonhals, *Broadband Dielectric Spectroscopy*, Springer, Berlin Heidelberg, 2012.
27 J. C. Lagarias, J. A. Reeds, M. H. Wright and P. E. Wright, *SIAM J. Optimiz.*, 1998, **9**, 112–147.
28 T. M. Inc., *MATLAB version: 9.11.0.1873467 (R2021b) Update 3*, 2021, https://www.mathworks.com.
29 A. Sanz, A. Linares, M. C. García-Gutiérrez, A. Nogales, S. Paszkiewicz, A. Zubkiewicz, A. Szymczyk and T. A. Ezquerra, *Front. Chem.*, 2022, **10**, 921787.
30 T. Blythe and D. Bloor, *Electrical Properties of Polymers*, Cambridge University Press, Cambridge, 2nd edn, 2008.
31 P. B. Ishai, M. S. Talary, A. Caduff, E. Levy and Y. Feldman, *Meas. Sci. Technol.*, 2013, **24**, 102001.
32 A. Nogales, A. Sanz, I. Šics, M.-C. García-Gutiérrez and T. A. Ezquerra, in *Order and Segmental Mobility in Crystallizing Polymers*, ed. G. Reiter and G. R. Strobl, Springer Berlin Heidelberg, Berlin, Heidelberg, 2007, pp. 435–456.
33 E. Schlosser and A. Schönhals, *Colloid Polym. Sci.*, 1989, **267**, 963–969.
34 A. Nogales, T. A. Ezquerra, J. M. Garcia and F. J. Balta-Calleja, *J. Polym. Sci., Part B: Polym. Phys.*, 1999, **37**, 37–49.
35 A. Nogales, T. A. Ezquerra, F. Batallan, B. Frick, E. Lopez-Cabarcos and F. J. Balta-Calleja, *Macromolecules*, 1999, **32**, 2301–2308.
36 A. Sanz, A. Nogales, T. A. Ezquerra, N. Lotti, A. Munari and S. S. Funari, *Polymer*, 2006, **47**, 1281–1290.
37 A. Sanz, A. Nogales, T. A. Ezquerra, M. Soccio, A. Munari and N. Lotti, *Macromolecules*, 2010, **43**, 671–679.
38 A. Sanz, A. Nogales and T. A. Ezquerra, *Macromolecules*, 2010, **43**, 29–32.
39 H. Vogel, *Phys. Z.*, 1921, **22**, 645–646.
40 G. S. Fulcher, *J. Am. Ceram. Soc.*, 1925, **8**, 339–355.
41 G. Tammann, *J. Soc. Glass Technol.*, 1925, **9**, 166–185.
42 T. Hecksher, A. I. Nielsen, N. B. Olsen and J. C. Dyre, *Nat. Phys.*, 2008, **4**, 673.
43 A. Sanz and K. Niss, *J. Chem. Phys.*, 2017, **146**, 044502.
44 C. Angell, *Polymer*, 1997, **38**, 6261–6266.

45 G. Papamokos, T. Dimitriadis, D. N. Bikiaris, G. Z. Papageorgiou and G. Floudas, *Macromolecules*, 2019, **52**, 6533–6546.
46 X. Xu, J. F. Douglas and W.-S. Xu, *Soft Matter*, 2025, **21**, 2664–2685.
47 S. Napolitano, E. Glynos and N. B. Tito, *Rep. Prog. Phys.*, 2017, **80**, 036602.
48 G. Strobl, *The Physics of Polymers: Concepts for Understanding Their Structures and Behavior*, Springer, Berlin, Heidelberg, 3rd edn, 2007.
49 L. Genovese, M. Soccio, N. Lotti, A. Munari, A. Szymczyk, S. Paszkiewicz, A. Linares, A. Nogales and T. A. Ezquerra, *Phys. Chem. Chem. Phys.*, 2018, **20**, 15696–15706.
50 A. Nogales, A. Sanz and T. A. Ezquerra, *J. Non-Cryst. Solids*, 2006, **352**, 4649–4655.
51 B. Jakobsen, K. Niss, C. Maggi, N. B. Olsen, T. Christensen and J. C. Dyre, *J. Non-Cryst. Solids*, 2011, **357**, 267–273.
52 P. Lunkenheimer and A. Loidl, in *Glassy Dynamics: From Millihertz to Terahertz*, ed. F. Kremer and A. Loidl, Springer International Publishing, Cham, 2018, pp. 23–59.
53 A. Nogales, A. Sanz, T. A. Ezquerra, R. Quintana and S. Munoz-Guerra, *Polymer*, 2006, **47**, 7078–7084.
54 A. Sanz, A. Nogales, N. Lotti, A. Munari and T. Ezquerra, *J. Non-Cryst. Solids*, 2007, **353**, 3989–3995.
55 S. Glasstone, K. J. Laidler and H. Eyring, *The Theory of Rate Processes*, McGraw-Hill, New York, 1941.
56 J. P. Crine, *J. Macromol. Sci., Part B: Phys.*, 1984, **23**, 201–219.
57 S. Sharifi, I. Asenjo-Sanz, J. A. Pomposo and A. Alegria, *Macromolecules*, 2022, **55**, 3627–3636.
58 D. Heczko, M. Tarnacka, K. Kaminski, M. Paluch and E. Kaminska, *J. Mol. Liq.*, 2023, **376**, 121377.
59 V. N. Novikov and A. P. Sokolov, *Entropy*, 2022, **24**, 1101.
60 J. C. Dyre, *J. Phys. C-Solid State Phys.*, 1986, **19**, 5655.
61 A. Schöenhals, D. Wolff and J. Springer, *Macromolecules*, 1995, **28**, 6254–6257.
62 L. Liu and Q.-X. Guo, *Chem. Rev.*, 2001, **101**, 673–696.
63 E. Thoms and S. Napolitano, *J. Chem. Phys.*, 2023, **159**, 161103.
64 R. Zorn, P. Szymoniak, M. A. Kolmangadi, R. Malpass-Evans, N. B. McKeown, N. H. Jalarvo, M. Tyagi, M. Böhning and A. Schönhals, *Soft Matter*, 2024, **20**, 5153–5163.
65 A. Zubkiewicz, A. Szymczyk, R. J. Sablong, M. Soccio, G. Guidotti, V. Siracusa and N. Lotti, *Polym. Degrad. Stab.*, 2022, **195**, 109800.
66 K. Niss, C. Dalle-Ferrier, G. Tarjus and C. Alba-Simionesco, *J. Phys.: Condens. Matter*, 2007, **19**, 076102.
67 P. Lunkenheimer, F. Humann, A. Loidl and K. Samwer, *J. Chem. Phys.*, 2020, **153**, 124507.
68 A. Tölle, H. Schober, J. Wuttke, O. G. Randl and F. Fujara, *Phys. Rev. Lett.*, 1998, **80**, 2374–2377.
69 G. Tarjus, D. Kivelson, S. Mossa and C. Alba-Simionesco, *J. Chem. Phys.*, 2004, **120**, 6135–6141.
70 R. Casalini and C. M. Roland, *Phys. Rev. Lett.*, 2014, **113**, 085701.
71 H. Hansen, A. Sanz, K. Adrjanowicz, B. Frick and K. Niss, *Nat. Commun.*, 2018, **9**, 518.
72 A. Sanz, T. Hecksher, H. W. Hansen, J. C. Dyre, K. Niss and U. R. Pedersen, *Phys. Rev. Lett.*, 2019, **122**, 055501.
73 T. Merkel, B. Freeman, R. Spontak, Z. He, I. Pinnau, P. Meakin and A. Hill, *Science*, 2002, **296**, 519–522.
74 S. K. Burgess, J. E. Leisen, B. E. Kraftschik, C. R. Mubarak, R. M. Kriegel and W. J. Koros, *Macromolecules*, 2014, **47**, 1383–1391.
75 J. Dudowicz, K. F. Freed and J. F. Douglas, *Generalized Entropy Theory of Polymer Glass Formation*, John Wiley and Sons, Ltd, 2008, ch. 3, pp. 125–222.
76 K. L. Ngai and C. M. Roland, *Macromolecules*, 1993, **26**, 6824–6830.
77 P. G. Santangelo and C. M. Roland, *Macromolecules*, 1998, **31**, 4581–4585.
78 K. Kunal, C. G. Robertson, S. Pawlus, S. F. Hahn and A. P. Sokolov, *Macromolecules*, 2008, **41**, 7232–7238.
79 A. Sanz, H. C. Wong, A. J. Nedoma, J. F. Douglas and J. T. Cabral, *Polymer*, 2015, **68**, 47–56.
80 A. Sanz, *Macromolecules*, 2011, **44**, 8124–8128.
81 P. A. Klonos, N. D. Bikiaris, A. Zamboulis, M. A. Valera, A. Mangas, A. Kyritsis and Z. Terzopoulou, *Soft Matter*, 2023, **19**, 7846–7858.
82 Q. Ma, Y. Wang, Y. Gu, N. Zhao, S. Luo, L. Wang, Y. Hu and J. Fang, *AIP Adv.*, 2022, **12**, 015207.
83 P. G. Debenedetti and F. H. Stillinger, *Nature*, 2001, **410**, 259–267.
84 J. C. Dyre, N. B. Olsen and T. Christensen, *Phys. Rev. B:Condens. Matter Mater. Phys.*, 1996, **53**, 2171–2174.
85 A. Yelon and B. Movaghar, *Phys. Rev. Lett.*, 1990, **65**, 618–620.
86 A. Yelon, B. Movaghar and H. M. Branz, *Phys. Rev. B: Condens. Matter Mater. Phys.*, 1992, **46**, 12244–12250.
87 R. P. White, S. Napolitano and J. E. G. Lipson, *Phys. Rev. Lett.*, 2025, **134**, 098203.
88 A. Zubkiewicz, A. Sanz, T. A. Ezquerra and A. Szymczyk, Dielectric Relaxation and Random Copolyesters. The Materials Data Facility, 2025, DOI: 10.18126/k1d9-3g72.

